Article

Not peer-reviewed version

Biogenic Selenium Nanoparticles from Food-Grade *Pediococcus acidilactici* JD-21: Selenite Bioreduction, Enhanced Probiotic Traits, and Antioxidant Protection

Shiyue Fan †, Jiaxu Li †, Xin Zhao †, Yi He, Zhiwei Li, Zhangqian Wang, Chao Gao, Ying Ma, Jinquan Li, Xiaoling Chen, Wen Cheng, Xingxing Dong *

Posted Date: 2 June 2026

doi: 10.20944/preprints202606.0122.v1

Keywords: *Pediococcus acidilactici* JD-21; selenium nanoparticles (SeNPs); selenite reduction; selenium-enriched probiotics; transcriptomic response

 doi:10.20944/preprints202606.0122.v1

Article

Biogenic Selenium Nanoparticles from Food-Grade *Pediococcus acidilactici* JD-21: Selenite Bioreduction, Enhanced Probiotic Traits, and Antioxidant Protection

Shiyue Fan [1,†], Jiaxu Li [1,†], Xin Zhao [1,†], Yi He [1], Zhiwei Li [2], Zhangqian Wang [1], Chao Gao [1], Ying Ma [1], Jinquan Li [3], Xiaoling Chen [1], Wen Cheng [4] and Xingxing Dong [1,*]

[1] National R&D Center for Se-rich Agricultural Products Processing, Hubei Engineering Research Center for Deep Processing of Green Se-rich Agricultural Products, School of Modern Industry for Selenium Science and Engineering, Wuhan Polytechnic University, Wuhan 430023, China

[2] Joint International Research Laboratory of Animal Health and Animal Food Safety, College of Veterinary Medicine, Southwest University, Chongqing 400715, China

[3] National Key Laboratory of Agricultural Microbiology, Huazhong Agricultural University, Wuhan 430070, China

[4] Hengfeng Wanda (Hubei) Pharmaceutical Technology Co., Ltd., Wuhan 430299, Hubei, China

* Correspondence: dongxingxinghg@163.com

† These authors contributed equally to this work.

Abstract

Selenite bioreduction by food-grade lactic acid bacteria enables mild production of selenium nanoparticles (SeNPs) together with selenium-enriched biomass. Here, a highly Se(IV)-tolerant isolate from Enshi soil was identified as *Pediococcus acidilactici* JD-21, which efficiently reduced 5 mmol/L Se(IV) and accumulated mainly ~60 nm protein/polysaccharide-capped SeNPs. Selenium enrichment markedly enhanced the antibacterial activity of JD-21 against *Escherichia coli*, *Staphylococcus aureus* and *Salmonella enteritidis* and improved survival in simulated gastric juice, indicating probiotic potential. In a mouse Streptococcus suis infection model, oral SeNPs alleviated infection-associated weight loss, restored antioxidant enzyme activities and reduced liver and spleen lesions. RNA-seq revealed 537 Se(IV)-responsive genes, with up-regulated redox, lipid/exopolysaccharide and transport pathways and down-regulated growth-related functions. These findings demonstrate that JD-21 is a promising food-grade chassis for producing biogenic SeNPs and selenium-enriched probiotics for selenium fortification and foodborne pathogen control.

Keywords: *Pediococcus acidilactici* JD-21; selenium nanoparticles (SeNPs); selenite reduction; selenium-enriched probiotics; transcriptomic response

1. Introduction

Selenium (Se) is an essential trace element that plays crucial roles in antioxidant defense, immune regulation, and maintenance of redox homeostasis in humans and animals. However, the biological activity and toxicity of selenium depend largely on its chemical form. Inorganic selenium species such as selenite (SeO_3^{2-}) and selenate (SeO_4^{2-}) are highly toxic at elevated concentrations, whereas organic selenium compounds and nanosized elemental selenium (Se^0) exhibit high bioavailability and low toxicity[1,2]. Hence, transforming inorganic selenium into safer and more bioavailable forms through green biological approaches has become an important research focus in food chemistry, nutrition, and microbial biotechnology.

 doi:10.20944/preprints202606.0122.v1

Microbial reduction of selenite to Se^0 or selenium nanoparticles (SeNPs) provides an environmentally friendly strategy for selenium detoxification and utilization. A variety of microorganisms, including bacteria, fungi, and yeasts, are capable of such conversions, but lactic acid bacteria (LAB) have gained increasing attention because of their Generally Recognized as Safe (GRAS) status and broad use in fermented foods[3,4]. Selenium-enriched LAB not only convert toxic inorganic selenium into biologically active forms but also enhance the nutritional and functional quality of food products and probiotic preparations[5,6]. Compared with environmental bacteria such as Pseudomonas or Bacillus, LAB-based selenium transformation is milder, safer, and more suitable for food applications[7].

Recent studies have revealed that several LAB species can reduce selenite to SeNPs or incorporate selenium into organic molecules. For example, *Lactobacillus casei* ATCC 393 was shown to reduce Se(IV) via a glutathione (GSH)-dependent redox pathway involving glutathione reductase and nitrate reductase[8]. *Lactiplantibacillus plantarum* NML21 demonstrated the capacity to produce uniform spherical SeNPs with high selenium tolerance[9]. Similarly, *Lactobacillus paralimentarius* JZ07 generated red SeNPs (150–300 nm) under Se(IV) stress, with carboxyl and amide groups on cell-surface polymers participating in selenium adsorption and nucleation[10]. Other studies have highlighted the importance of extracellular polymeric substances (EPS) and surface proteins in stabilizing SeNPs[11,12]. Furthermore, selenium-enriched LAB strains such as *Pediococcus acidilactici* MRS-7 and *Lactiplantibacillus plantarum* S14 have exhibited strong antioxidant and antimicrobial properties and improved survival in gastrointestinal conditions[6,13]. At the systems level, multi-omics analyses have begun to unravel selenium-responsive regulatory networks in LAB, indicating the involvement of redox-active enzymes, thiol metabolism, and stress-related signaling pathways[14,15]. Moreover, animal studies have shown that SeNPs can enhance antioxidant status, modulate immune or inflammatory responses, and protect against oxidative stress-related tissue injury, supporting the need for in vivo evaluation of their functional activity[16–18].

Although these studies have provided valuable insights into the selenium conversion ability of LAB, the current understanding of how LAB adapt to and tolerate high concentrations of selenite remains limited. Most reported strains can only withstand relatively low Se levels, and few studies have systematically examined the coordinated molecular responses underlying selenium reduction and tolerance. Additionally, the relationship between intracellular redox regulation, SeNPs formation, and probiotic functionality is still unclear. Addressing these questions is essential to better harness LAB as efficient and safe microbial platforms for selenium biofortification and functional food development.

In this context, we isolated a highly selenium-tolerant strain, *Pediococcus acidilactici* JD-21, capable of reducing high concentrations of sodium selenite to red SeNPs. This study systematically investigated its selenium transformation characteristics, nanoparticle morphology, probiotic properties, and safety. Furthermore, transcriptomic analysis was performed to explore the molecular responses to selenium stress. The findings of this work provide new evidence for understanding selenium metabolism and adaptive mechanisms in LAB and contribute to the rational application of selenium-enriched probiotics in food and health industries.

2. Materials and Methods

2.1. Isolation and Identification of Selenite-Reducing Strains

All strains were originally isolated from seleniferous soils sampled from Enshi County, Hubei Province, China, which is reputed as “The World Capital of Selenium”. Briefly, 10 g of soil sample was suspended in 90 mL phosphate-buffered saline (PBS). Under the shaking of 200 rpm for 30min at 30 ℃ and then under static condition for 5 min. The upper suspension was centrifuged at 5,000 rpm for 15 min, and the pellets were suspended in 10 mL PBS. Then 1mL suspension was inoculated in 50 mL De Man, Rogosa and Sharpe medium (MRS medium，Qingdao High-tech Industrial Park Haibo Biotechnology Co., Ltd) and incubated for 6 h at 37 °C with shaking at 180 rpm. The enrichment

 doi:10.20944/preprints202606.0122.v1

culture was serially diluted and spread on MRS agar and incubated for 48h at 37 °C. All strains were further purified by streak plating, and then preliminarily identified and were numbered based on their morphological. The 16S rDNA sequencing analysis was performed to identify all isolates and was conducted in Sangon Biotechnology Co., Ltd. (Shanghai, China). The sequence was compared with all the available sequences in GenBank database with Basic Local Alignment Search Tool (BLAST) program (http://blast.ncbi.nlm.nih.gov). Multiple sequence alignment of 16S rRNA gene sequences was performed using ClustalW implemented in MEGA-X (version 10.0.5). A phylogenetic tree was constructed using the neighbor-joining (NJ) method with 1,000 bootstrap replications to assess the reliability of the branches.

2.2. Growth and Biotransformation of JD-21 Under Se(IV) Stress

The isolates were inoculated in MRS medium containing concentrations of selenite (0, 5, 10, 25, 50, and 100 mmol/L) and incubated for 36 h at 37 °C. The maximum concentration at which red SeNPs were produced was identified as the selenite tolerance limit. To determine the effect of selenium on the growth of the strain, the optical density (OD) of the strain's fermentation broth was measured every three hours at a wavelength of 600 nm using a UV spectrophotometer. Each group repeated three times.

To determine the selenium reduction efficiency of the strain, strain JD-21 was inoculated in MRS medium containing 5 mmol/L Na_2SeO_3 and incubated at 37 °C and 180 rpm for 72 h. Samples were taken every 12 h, centrifuged at 12,000 rpm for 20 minutes, the supernatant was digested with HNO_3, and finally the samples were diluted. The selenium content in the supernatant was determined by Inductively coupled plasma-mass spectrometry (ICP-MS, Agilent 1290II-8900, Agilent Technologies Co., Ltd)[19,20].

$$Reduction\ rate(\%) = [1 - \frac{(((P - P_0) \times V/1000 \times f)/v)}{865}] \times 100$$

where P and P_0 is the mass concentration of Se element in the sample solution and the blank solution, μg/L; V is the volume of the sample digestion liquid to be made up to volume, mL; f is the dilution factor of the sample, v is the volume of sample, mL; 865 is the initial concentration of sodium selenite, μg/mL.

2.3. Subcellular Localization and Structural Characterization of Selenium Nanoparticle Biosynthesis

To determine the subcellular localization of selenium nanoparticles (SeNPs) biosynthesis, the assay was conducted according to Huang et al.[21] with minor modifications. Subcellular fractions, including periplasmic proteins, cytoplasmic extracts, cell membrane components, extracellular polysaccharides, and culture supernatants, were prepared and used as potential SeNPs-producing sources. A reaction mixture consisting of 100 μL of each fraction, 88 μL of McIlvaine buffer, 10 μL of Na_2SeO_3 solution, and 2 μL of NADH was dispensed into 96-well plates and incubated at 37 °C for 48 h. The appearance of a red coloration indicated the formation of elemental selenium (Se^0), suggesting that the corresponding subcellular fraction served as the primary site of SeNP synthesis.

To further validate the subcellular localization results and characterize the morphology and surface functional groups of the biosynthesized SeNPs, scanning electron microscopy (SEM) and Fourier Transform Infrared Spectroscopy (FT-IR) analysis were subsequently performed. The strain was cultured in MRS supplemented with 5 mmol/L Na_2SeO_3 at 37 ℃ and 180 rpm for 48 h, followed by centrifugation at 12,000 rpm for 10 min to collect the bacterial cells. A part of the precipitated cells was disrupted using a ultra-high-pressure low temperature cell disruptor (JN-MINIPRO, Guangzhou Juneng Nano & Bio Technology Co., Ltd) at 4 ℃ under 1500 MPa. The resulting suspension was centrifuged again (12,000 rpm, 10 min), and the pellet (non-disrupted and disrupted) was fixed with 2.5% glutaraldehyde at 4 °C overnight. For FT-IR analysis, another portion of the bacterial culture was freeze-dried, ground, and homogenized with potassium bromide (KBr) to form transparent pellets. The samples were then subjected to FT-IR spectral scanning in the range of 400–4000 cm^{-1}[21].

 doi:10.20944/preprints202606.0122.v1

2.4. Determination of Total Selenium and Selenium Speciation

Strain JD-21 was inoculated into MRS supplemented with 5 mmol/L Na_2SeO_3 and incubated at 37 °C for 24 h and 48 h. The cultured cells were harvested by centrifugation (8,000 rpm, 10 min), washed three times with sterile saline, and freeze-dried under vacuum (LGJ-25, Beijing Sihuan Qihang Technology Co., Ltd). For total selenium determination, 0.05 g of lyophilized biomass was digested with HNO_3, diluted to an appropriate volume, and quantified using Liquid chromatography–atomic fluorescence spectrometry (LC-AFS8530, Haiguang Instrument Co., Ltd)[22].

For selenium speciation analysis, 0.1 g of the dried sample was resuspended in sterile water and disrupted using an ultra-high-pressure low temperature cell disruptor. Subsequently, 2 mL of the lysate was mixed with 1 mL of hydrolysate containing 2 mg protease E and incubated at 37 °C for 24 h, followed by ultrasonication for 30 min. After centrifugation (8,000 rpm, 10 min), the supernatant was collected and filtered through a 0.22 μm nylon membrane. Selenium species were then identified and quantified using high-performance liquid chromatography coupled with inductively coupled plasma mass spectrometry (HPLC-ICP-MS). The Se species were identified according to the retention time of Se standard substances including $SeCys_2$, MeSeCys, Se(IV), SeMet and Se (VI). The working parameters and elution gradients were listed in Supplementary Materials Table S1[23].

2.5. Antimicrobial Activity of Selenium-Enriched JD-21 Cultures

Strain JD-21 was inoculated into MRS with or without 5 mmol/L Na_2SeO_3 and incubated at 37 °C with shaking at 180 rpm for 24 h. Pathogenic strains (*Escherichia coli* ATCC 18683, *Staphylococcus aureus* ATCC 6538 and *Salmonella enteritidis* ATCC 13076) were harvested from fresh agar plates, resuspended in PBS, and adjusted to an optical density at 600 nm (OD_{600}) of 0.5. For the agar diffusion assay, 15 mL of LB agar was poured into a sterile Petri dish to form the base layer. After solidification, three sterile Oxford cups were placed on the agar surface. Subsequently, 5 mL of LB agar containing 1%(v/v) of the standardized pathogen suspension was poured onto the base layer. After solidification, Oxford cups were pulled out. One well was filled with 200 μL sterile MRS medium (negative control), and the remaining wells were filled with 200 μL of JD-21 culture without selenium, selenium-enriched JD-21 culture, respectively. Plates were incubated at 37 °C for 24 h, and the inhibition zones around each well were then recorded[22,24].

2.6. Survival of Selenium-Enriched JD-21 in Simulated Gastric Juice

Pepsin was dissolved in sterile PBS adjusted to pH 3.0 to prepare simulated gastric juice containing 3 g/L pepsin, and the solution was sterilized by filtration through a 0.22 μm membrane filter. Strain JD-21 was cultured in MRS at 37 °C for 12 h. Then, 1 mL of the JD-21 culture was inoculated into 9 mL of the simulated gastric juice and incubated at 37 °C with shaking at 90 rpm for 3 h. Viable cell counts at 0 h and 3 h were determined by plate counting on MRS agar after appropriate serial dilutions. The survival rate was calculated according to the following equation[21,25]:

$$\text{Survival rate}(\%) = (1 - \frac{N_{3h}}{N_{0h}}) \times 100$$

where N_{0h} and N_{3h} epresent the viable counts (CFU/mL) of JD-21 at 0 h and 3 h, respectively.

2.7. In Vivo Anti-Infective Activity of SeNPs Against Streptococcus Suis

Male mice (n = 8 per group) were randomly assigned to four groups: (1) control group, (2) SeNPs group, (3) *S. suis* infection group, and (4) SeNPs + *S. suis* treatment group. Mice in the SeNPs group and SeNPs + *S. suis* treatment group received SeNPs by oral gavage at a dose of 1.0 mg SeNPs/kg body weight once daily for 15 consecutive days, while the control and *S. suis* infection group were administered with an equal volume of water. On day 8, each mouse in the *S. suis* infection group and SeNPs + *S. suis* treatment group was inoculated by intraperitoneal injection with 0.2 mL of a *Streptococcus suis* suspension in PBS (6×10^9 CFU/mL). All animals were maintained under controlled

 doi:10.20944/preprints202606.0122.v1

environmental conditions (25 ± 2 °C, 12 h light/dark cycle) with free access to standard chow and water. Feed intake was recorded daily at the same time, and clinical signs, including responsiveness, general appearance, mental state, and coat condition, were monitored throughout the experiment. Body weight was measured every two days[26]. At the end of the experiment, blood samples were collected, and the mice were euthanized. Serum, liver, and spleen tissue homogenates were prepared, and the activities of superoxide dismutase (SOD), total antioxidant capacity (T-AOC), and glutathione peroxidase (GSH-Px) were determined using commercial ELISA kits according to the manufacturers' instructions. For histopathological analysis, liver and spleen tissues were fixed in 4% (w/v) paraformaldehyde, dehydrated through a graded ethanol series, embedded in paraffin, sectioned, and stained with hematoxylin and eosin (H&E) for microscopic examination[5]. The present study was conducted in strict accordance with the ethical standards for animal experimentation. The animal study protocol was reviewed and approved by the Animal Ethics Committee of Wuhan Myhalic Biotechnology Co., Ltd. (protocol code: HLK 20230921-004; date of approval: September 21, 2023). Throughout the research, we upheld the highest standards of animal care and welfare, ensuring that all procedures were consistent with national and international guidelines on humane treatment of animals. This included the implementation of measures to alleviate pain and distress, such as appropriate use of anesthesia and analgesia, as well as the application of the 3Rs principle—Replacement, Reduction, and Refinement—to optimize scientific rigor while minimizing animal usage.

2.8. Comparative Transcriptomic Analysis of JD-21 by RNA-seq

JD-21 was cultivated in MRS supplemented with or without 5 mmol/L Na_2SeO_3, and cells were harvested after 7 h of incubation for comparative transcriptomic analysis. Total RNA was extracted from each sample using a Total RNA Isolation Kit (Sangon Biotech, Shanghai, China) according to the manufacturer's instructions. RNA concentration and purity were assessed with a NanoDrop spectrophotometer (Thermo Fisher Scientific, USA). High-quality RNA samples were used for library construction, and sequencing was performed on an Illumina HiSeq platform (Novogene, Beijing, China). Raw sequencing reads were subjected to quality control and filtering with SOAPnuke to remove adaptor sequences, low-quality reads, and reads containing ambiguous bases, yielding high-quality clean reads. Clean reads were then aligned to the JD-21 reference genome using SOAP2 (v2.2.1), and gene-level read counts were obtained for subsequent analysis. Differentially expressed genes (DEGs) between selenium-supplemented and control cultures were identified using the edgeR package in R. Genes with a false discovery rate (FDR) < 0.05 and an absolute $\log_2$ fold change ($|\log_2 FC|$) > 1 were considered significantly differentially expressed. Functional annotation and enrichment analyses of DEGs were performed based on the Gene Ontology (GO) and Kyoto Encyclopedia of Genes and Genomes (KEGG) databases[15,27].

2.9. Statistical Analysis

Statistical analyses were performed using GraphPad Prism 8.3.0 software (GraphPad Software, San Diego, CA, USA). Data are presented as the mean ± standard error of the mean (SEM). The normality of data distribution and homogeneity of variance were assessed before statistical analysis. For comparisons between two groups, an unpaired two-tailed Student's t-test was used when the data were normally distributed and showed equal variances. For comparisons among multiple groups, one-way analysis of variance (ANOVA) followed by an appropriate post hoc test was performed. When the data did not meet the assumptions of normality or equal variance, non-parametric tests, including the Mann–Whitney U test for two-group comparisons and the Kruskal–Wallis test for multiple-group comparisons, were used. All statistical tests were two-tailed, and $p < 0.05$ was considered statistically significant.

 doi:10.20944/preprints202606.0122.v1

3. Results and discussion

3.1. Isolation and Identification of the Se(IV)-Reducing Strain JD-21

A total of 70 isolates were obtained from soil samples collected in Enshi. Among these, one isolate formed milky-white, round colonies with a smooth and moist surface on MRS agar (Figure 1A). When grown on MRS plates supplemented 5 mmol/L Na_2SeO_3, the colony size showed no obvious change, whereas the colony color gradually shifted from milky white to red (Figure 1B). This selenite-induced red pigmentation suggested the in situ formation of elemental selenium nanoparticles (SeNPs)[28]. This strain was designated JD-21. 16S rRNA gene sequence analysis showed that JD-21 shared 99.66% similarity with *Pediococcus acidilactici*. Phylogenetic analysis based on the 16S rRNA gene clustered JD-21 together with *P. acidilactici* strains (Figure 1C), supporting its identification as *P. acidilactici*. This strain has been deposited in the China Center for Type Culture Collection (CCTCC) under the accession number CCTCC M 20241452.

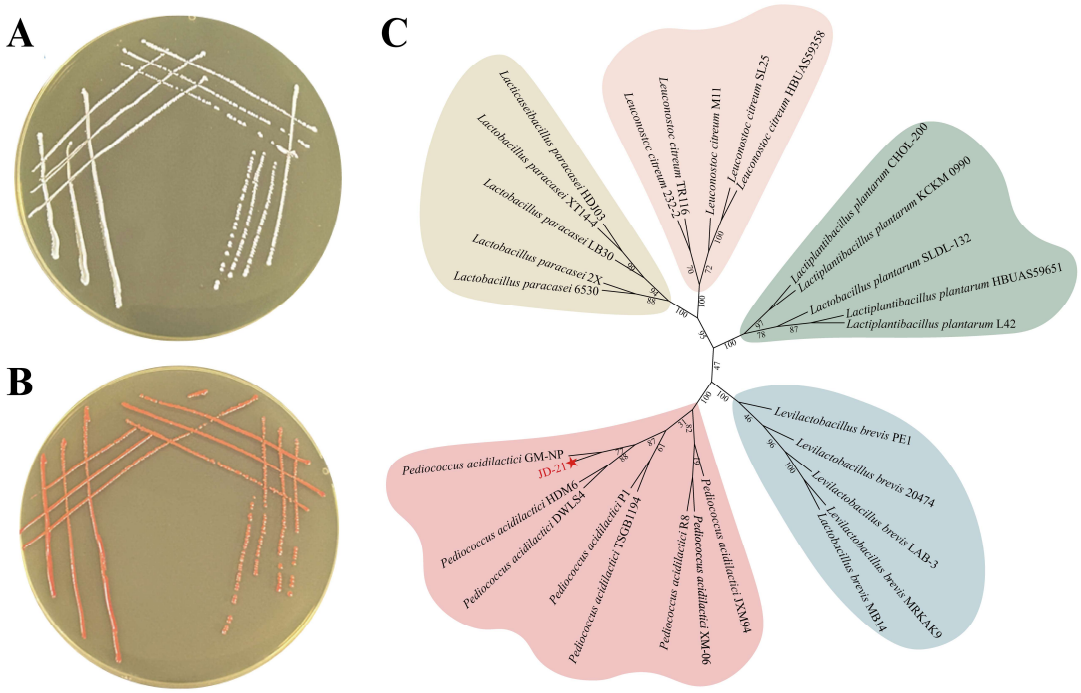

Figure 1. Colony morphology of strain JD-21 on (A) MRS agar and (B) MRS agar supplemented with 5 mmol/L Na_2SeO_3, showing selenite-induced red pigmentation. (C) Phylogenetic tree of JD-21 based on 16S rRNA gene sequences.

3.2. Growth and Biotransformation of JD-21 Under Se(IV) Stress

Among the 70 isolates obtained from Enshi soil, 22 strains exhibited Se(IV) tolerance at Na_2SeO_3 concentrations higher than 25 mmol/L. JD-21 showed the strong tolerance, being able to grow in the presence of up to 100 mmol/L Na_2SeO_3, and was therefore selected for further investigation as a highly Se(IV)-tolerant strain of *Pediococcus acidilactici*. When JD-21 was cultivated on MRS agar containing 5 mmol/L Na_2SeO_3, dark-red precipitates appeared and the cells became pigmented (Figure 2A), indicating that the strain reduced Se(IV) to red elemental selenium[10].

As shown in Figure 2B, JD-21 reached its maximal growth at approximately 14 h in MRS without Na_2SeO_3. At low Na_2SeO_3 concentrations, the growth of JD-21 was not markedly affected compared with the control. In contrast, 25 mmol/L Na_2SeO_3 caused a slight delay and reduction in growth, and 50 mmol/L Na_2SeO_3 markedly inhibited cell proliferation, indicating that high Se(IV) levels exert an

 doi:10.20944/preprints202606.0122.v1

inhibitory effect on JD-21. Considering both Se(IV) tolerance and growth performance, 5 mmol/L Na_2SeO_3 was selected as the working concentration for subsequent experiments. The time course of Se(IV) reduction by JD-21 is shown in Figure 2C. The proportion of Se(IV) removed from the medium increased progressively with incubation time, reaching a maximum at 72 h, when 60.85% of the initial selenite had been converted into other selenium species. Previously reported probiotic strains typically show Se(IV) reduction rates of approximately 20–70% at relatively low Na_2SeO_3 concentrations, most often below 3 mmol/L[3]. These results indicate that JD-21 combines a relatively high Se(IV) reduction capacity with Se(IV) tolerance far exceeding 3 mmol/L, highlighting its potential as a Se(IV)-resistant, SeNPs-producing probiotic candidate.

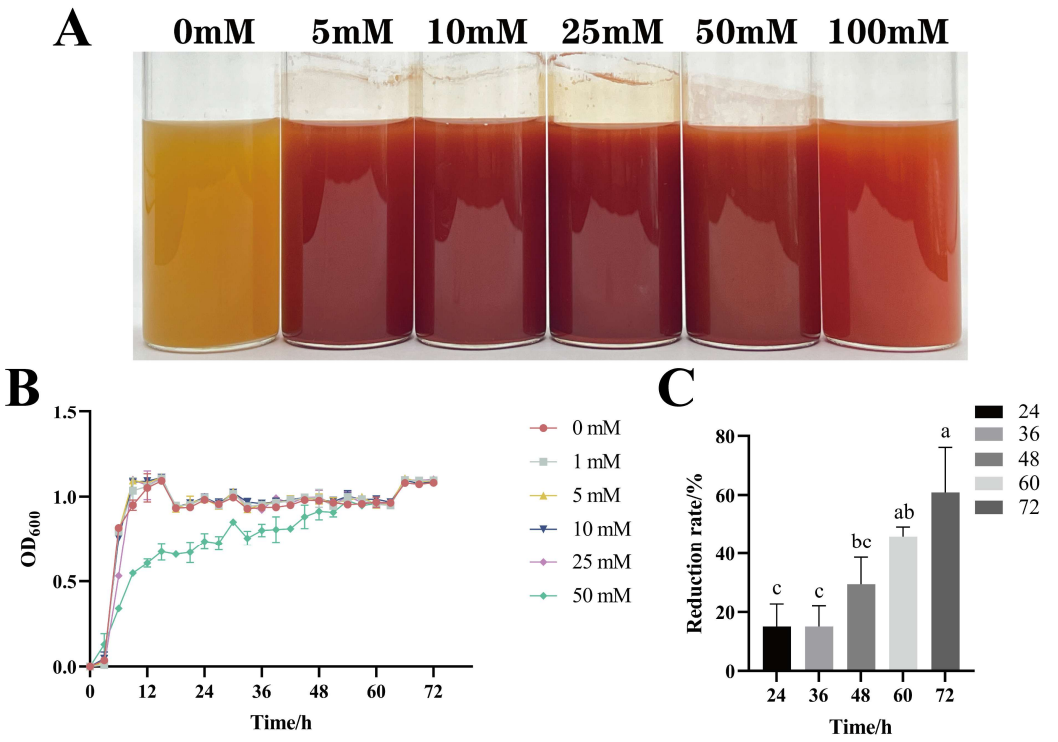

Figure 2. Effect of Se(IV) on the growth and Se(IV)-reducing capacity of Pediococcus acidilactici JD-21. (A) Effect of different Na_2SeO_3 concentrations (5, 10, 25, 50, and 100 mmol/L) on the growth of JD-21 in MRS medium. (B) Growth curves of JD-21 in MRS supplemented with 0, 1, 5, 10, 25, and 50 mmol/L Na_2SeO_3. (C) Time-dependent reduction of 5 mmol/L Na_2SeO_3 by JD-21 over 72 h.

3.3. Selenium Accumulation and Intracellular Speciation in JD-21

The selenium enrichment capacity of JD-21 during fermentation was first evaluated by measuring the total selenium content in *Pediococcus acidilactici* biomass. As shown in Figure 3A, in the 5 mmol/L Na_2SeO_3 treatment group, the selenium content of JD-21 pellets reached 64 177.33 ± 7 523.56 μg/g (≈ 64.18 mg/g, dry weight) at 24 h and further increased to 96 812.00 ± 7 261.33 μg/g (≈ 96.81 mg/g) at 48 h, indicating highly efficient selenium accumulation under these conditions. Previous studies have reported that *Lactiplantibacillus plantarum* 6076 and *Lactococcus lactis* 23185 accumulated 4.88 ± 0.39 mg/g and 3.68 ± 0.23 mg/g selenium, respectively, when cultivated with 10 μg/mL Se[24]. These comparisons highlight JD-21 as a promising strain for the preparation of selenium-enriched probiotic biomass.

To further elucidate the intracellular forms of selenium, selenium speciation analysis was performed by HPLC-ICP-MS. As shown in Figure 3B, chromatographic separation of selenium standards resolved five species: selenocystine ($SeCys_2$, retention time 2.3 min), methylselenocysteine (MeSeCys, 2.8 min), Se(IV) as selenite (Se^{4+}, 3.3 min), selenomethionine (SeMet, 4.8 min), and Se(VI)

 doi:10.20944/preprints202606.0122.v1

as selenate (Se^{6+}, 9.8 min). In JD-21 cells cultivated with 1 mmol/L Na_2SeO_3 (Figure 3C), $SeCys_2$ and residual Se(IV) were the main detectable species in the soluble fraction. The $SeCys_2$ peak (around 2.3–2.5 min) corresponded to 0.1362 ± 0.0075 μg/g (dry weight), whereas the Se^{4+} peak at 3.3 min accounted for 0.5479 ± 0.0313 μg/g. When the Na_2SeO_3 concentration was increased to 5 mmol/L, the chromatographic profile of JD-21 (Figure 3D) was dominated by the Se^{4+} peak at 3.3 min, with a concentration of 2.3235 μg/g, while the $SeCys_2$ signal remained at a low level (approximately 0.1500 μg/g) without a marked increase. Given that the most frequently reported organic selenium species in lactic acid bacteria are SeMet and $SeCys_2$[29], these results suggest that under higher selenite stress a smaller fraction of Se(IV) is incorporated into low-molecular-weight organoselenium forms, and a larger proportion is likely reduced to insoluble or nanoparticulate selenium that is not recovered in the soluble fraction analyzed by HPLC-ICP-MS.

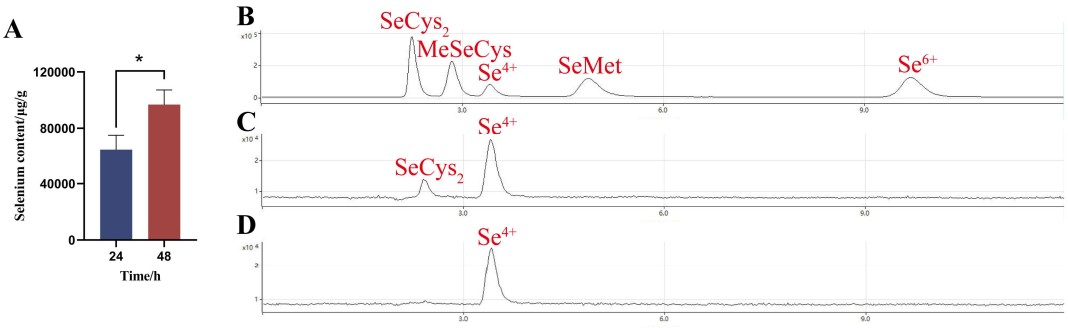

Figure 3. Selenium speciation and accumulation in Pediococcus acidilactici JD-21. (A) Total selenium content in JD-21 biomass after 24 h and 48 h of cultivation with 5 mmol/L Na_2SeO_3. (B) Selenium standard solution (80 μg/mL) containing $SeCys_2$, MeSeCys, Se(IV) (Se^{4+}, selenite), SeMet and Se(VI) (Se^{6+}, selenate). (C) Selenium speciation in JD-21 cells cultivated in MRS with 1 mmol/L Na_2SeO_3. (D) Selenium speciation in JD-21 cells cultivated in MRS with 5 mmol/L Na_2SeO_3.

3.4. Localization and Characterization of Selenium Nanoparticles

To determine the main cellular site of Se(IV) reduction in JD-21, cultures were fractionated into cytoplasmic and cell envelope–associated protein fractions, and the Se(IV)-reducing activity of each fraction was compared. The cytoplasmic fraction exhibited the highest Se(IV)-reducing activity, whereas the cell envelope-associated fraction showed only moderate activity (Figure 4A). The addition of exogenous NADH or NADPH did not markedly enhance the reduction rate in either fraction, suggesting that endogenous reducing equivalents are sufficient to support Se(IV) reduction under the tested conditions. These observations are consistent with previous findings that multiple enzymes located in different cellular compartments can participate in bacterial selenite reduction[30], and agree with reports of SeO_3^{2-}-reducing activity in the cytoplasmic protein fraction of Providencia rettgeri HF16[31].

The localization and morphology of JD-21–derived selenium nanoparticles were further examined by transmission electron microscopy (TEM). In cells grown with selenite, numerous electron-dense selenium nanoparticles were observed on the cell surface (Figure 4B). The cells remained plump and smooth with clear boundaries, indicating that selenium exposure did not cause obvious morphological damage to JD-21. After cell disruption, large numbers of selenium nanoparticles were visible on both the inner and outer surfaces of the cells (Figure 4C). These findings suggest that the primary reduction site of SeO_3^{2-} in *Pediococcus acidilactici* JD-21 is located in the cytoplasm, where Se(IV) is reduced to elemental selenium [Se(0)] by cytoplasmic and membrane-associated reductases, followed by nucleation and growth of selenium nanoparticles. The formed SeNPs are then redistributed to the cell surface, potentially via efflux systems, membrane transport processes, or cell lysis[9]. The SeNPs synthesized by JD-21 were predominantly spherical with a

 doi:10.20944/preprints202606.0122.v1

relatively uniform size distribution, with an average particle diameter of approximately 60 nm. Selenium nanoparticles with diameters below 200 nm are generally reported to exhibit enhanced biological effects, and smaller SeNPs often show higher biological activity. Wang et al.[9] further demonstrated that the antiproliferative activity of SeNPs against cancer cells is inversely related to particle size.

The surface functional groups associated with JD-21-derived selenium nanoparticles were analyzed by FT-IR by comparing cultures grown in selenium-free and selenium-containing media (Figure 4D). The broad band at 3292 cm^{-1} can be attributed to O-H and N-H stretching vibrations, indicating the presence of hydroxyl- and amino-containing biomolecules such as polysaccharides and proteins on the particle surface. The band at 2925 cm^{-1} corresponds to C-H stretching, which is typically associated with aliphatic chains in lipids and protein side chains. Characteristic bands at 1657 and 1537 cm^{-1} are assigned to amide I and amide II vibrations of proteins and peptides, while the band at 1231 cm^{-1}, together with the band at 1055 cm^{-1}, can be related to C-O and C-O-C stretching in polysaccharides or glycoproteins[13]. Compared with selenium-free cultures, selenium-enriched JD-21 samples showed stronger amide- and carbohydrate-related bands, suggesting that the biosynthesized SeNPs are capped and stabilized by protein- and polysaccharide-like biomolecules. These surface-bound biopolymers are likely to contribute to the colloidal stability and biological activity of the JD-21-derived selenium nanoparticles.

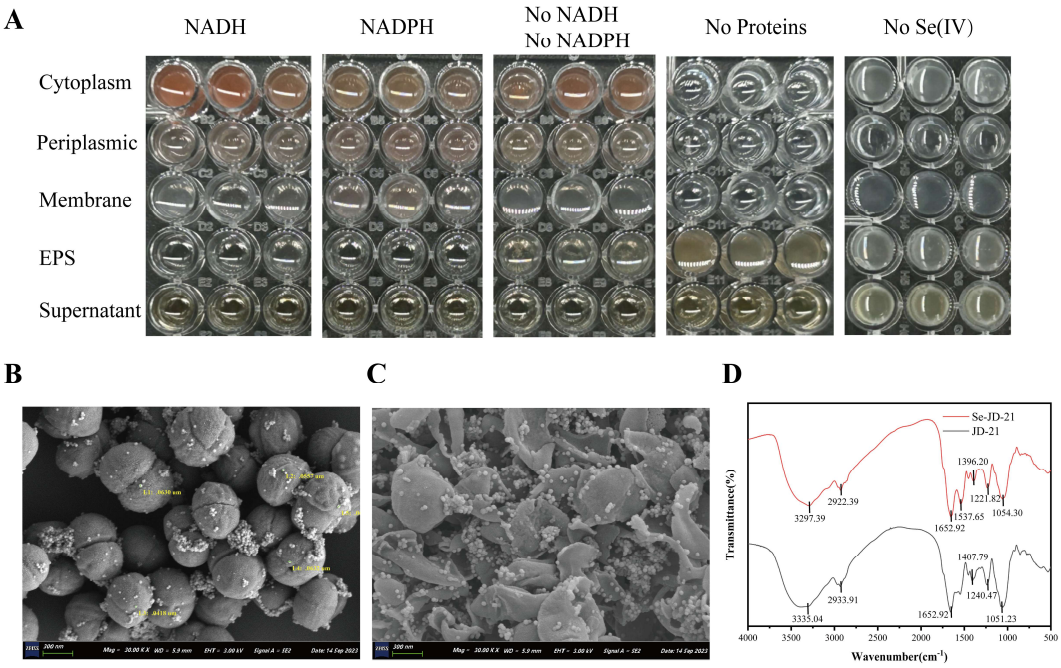

Figure 4. Localization and characterization of selenium nanoparticles produced by *Pediococcus acidilactici* JD-21. (A) Se(IV)-reducing activity in the cytoplasmic and cell envelope–associated protein fractions of JD-21 cultivated with 5 mmol/L Na_2SeO_3. (B) TEM image of intact JD-21 cells grown with selenite, showing selenium nanoparticles on the cell surface. (C) TEM image of JD-21 after cell disruption, revealing selenium nanoparticles associated with both the inner and outer cell surfaces. (D) Fourier transform infrared (FT-IR) spectra of JD-21 cultures grown in MRS broth with or without 5 mmol/L Na_2SeO_3.

3.5. Beneficial Properties of JD-21

To evaluate the antibacterial properties of JD-21 before and after selenium enrichment, three typical foodborne pathogenic bacteria were selected as indicator strains. The inhibition zones produced by Se-enriched JD-21 (Se-JD-21) and non-enriched JD-21 cultures against *Escherichia coli* were 32.15 ± 0.21 mm and 14.75 ± 0.35 mm, respectively. Against *Staphylococcus aureus*, the inhibition

 doi:10.20944/preprints202606.0122.v1

zones were 18.90 ± 0.17 mm for Se-JD-21 and 10.67 ± 0.29 mm for JD-21. For *Salmonella enteritidis*, Se-JD-21 and JD-21 produced inhibition zones of 29.83 ± 0.29 mm and 16.87 ± 0.23 mm, respectively. These results indicate that JD-21 exhibits inhibitory activity against all three pathogens, and that selenium enrichment markedly enhances its antibacterial effect (Figure 5A–C). Consistently, Yang et al.[32] reported that a selenium-enriched *Lactobacillus delbrueckii ssp. bulgaricus* (XN-L-Se) produced an inhibition zone of 18.05 ± 0.06 mm against *Staph. aureus* XN-SA, and that 12 μg/mL sodium selenite alone exhibited strong antibacterial activity, with an inhibition zone of 33.01 ± 0.22 mm. Together, these findings support the notion that selenium enrichment can enhance the antibacterial capacity of lactic acid bacteria.

The tolerance of JD-21 and Se-JD-21 to simulated gastric conditions was further assessed. After 3 h of exposure to artificial gastric juice, the survival rate of JD-21 was 61.54 ± 12.73%, whereas Se-JD-21 showed a significantly higher survival rate of 92.86 ± 8.25% (Figure 5D). Lv et al.[33] reported that sixteen lactic acid bacteria strains displayed survival rates of 50.95–73.23% in simulated gastric fluid and 40.01–52.98% in simulated intestinal fluid. In our study, both JD-21 and Se-JD-21 exhibited survival rates above 60% in simulated gastric juice, and selenium enrichment further improved acid tolerance. These results suggest that JD-21 possesses good resistance to gastric acidity and has promising potential as an intestinal probiotic candidate.

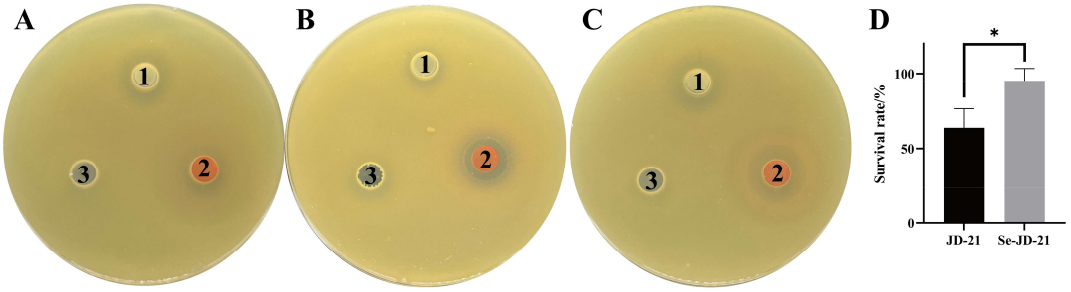

Figure 5. Antibacterial activity of JD-21 before and after selenium enrichment and survival under simulated gastric conditions. (A–C) Inhibition of three foodborne pathogens by culture supernatants of JD-21 and selenium-enriched JD-21 (Se-JD-21): (A) *Escherichia coli*, (B) *Staphylococcus aureus*, and (C) *Salmonella enteritidis*. 1, JD-21; 2, JD-21 cultivated with 5 mmol/L Na_2SeO_3 (Se-JD-21); 3, MRS medium control. (D) Survival of JD-21 and Se-JD-21 after 3 h of incubation in simulated gastric juice. Differences were considered statistically significant at $P < 0.05$.

3.6. Anti-Infective Activity of SeNPs Against Streptococcus Suis

To assess the health-related potential of selenium nanoparticles (SeNPs) in maintaining nutritional status and antioxidant balance during physiological stress, we evaluated growth performance (body weight and feed intake), systemic and tissue antioxidant activities (GSH-Px, SOD, and T-AOC in serum, liver, and spleen), as well as liver and spleen histomorphology (H&E staining) across the experimental groups.

Mice in the control group exhibited a progressive increase in body weight accompanied by a relatively stable pattern of feed intake over the experimental period (Figure 6 A), reflecting normal growth and nutritional status. The SeNPs group showed comparable trajectories, supporting that the gavaged SeNPs regimen was well tolerated and did not induce overt physiological disturbance. Following the day-8 challenge, the infection group displayed a pronounced deterioration in feeding behavior with a sharp decline in feed intake and a concomitant blunting of body-weight gain (Figure 6B), consistent with a stress-associated catabolic state that compromises nutrient intake and growth performance. Importantly, SeNPs treatment alleviated these adverse changes, as indicated by a less severe reduction in feed intake and a better maintenance of body-weight gain relative to the infection group. From a food-and-nutrition perspective, these outcomes suggest that SeNPs help sustain

 doi:10.20944/preprints202606.0122.v1

nutritional resilience—i.e., the capacity to maintain appetite and growth—under conditions that otherwise disrupt feeding and energy balance.

Biochemical indices further supported an SeNPs-associated improvement in antioxidant competence. The infection group showed depressed antioxidant enzyme activities and total antioxidant capacity across serum and metabolically active organs, with lower GSH-Px and SOD activities and reduced T-AOC compared with the non-challenged controls (Figure 6C–E). In contrast, SeNPs treatment significantly restored these redox-related indices in multiple compartments relative to the infection group (comparisons without “ns” indicating significance), indicating a reinforced enzymatic and non-enzymatic antioxidant network. This pattern is nutritionally meaningful because selenium is a key micronutrient linked to redox homeostasis, and GSH-Px—one of the most representative selenium-dependent antioxidant enzymes—plays a central role in detoxifying peroxides using glutathione as the reducing substrate. The elevation of GSH-Px, together with the improvement in SOD and T-AOC, suggests that SeNPs administration supports coordinated antioxidant defenses, which may translate into a lower oxidative burden and improved maintenance of physiological functions during stress[5].

Histopathological observations were consistent with the physiological and biochemical readouts (Figure 6F). Representative liver sections from the control and SeNPs groups displayed preserved hepatic architecture, with relatively regular hepatic cords and sinusoidal spaces and no obvious widespread structural disruption. In the infection group, liver morphology showed clear injury features, including increased structural disorganization and areas suggestive of inflammatory infiltration and/or vascular congestion, indicative of hepatic stress and impaired tissue homeostasis. Notably, the SeNPs treatment group exhibited an attenuated pathological phenotype relative to the infection group, with overall architecture appearing more preserved and fewer severe disruptive features, supporting the protective association suggested by the biochemical antioxidant improvements. Similarly, spleen sections from the control and SeNPs groups showed an intact overall organization, whereas the infection group demonstrated marked alterations consistent with inflammatory stress, including disturbed splenic architecture and more prominent red-pulp–associated changes, suggesting immune-related tissue perturbation. These changes were visibly mitigated in the SeNPs treatment group, which showed a trend toward restoration of splenic structural integrity compared with the infection group. Collectively, the concordance among growth/feeding performance, antioxidant indices, and tissue morphology supports the interpretation that SeNPs contribute to maintaining organ integrity and systemic physiological status, primarily through enhancing antioxidant capacity and redox buffering.

 doi:10.20944/preprints202606.0122.v1

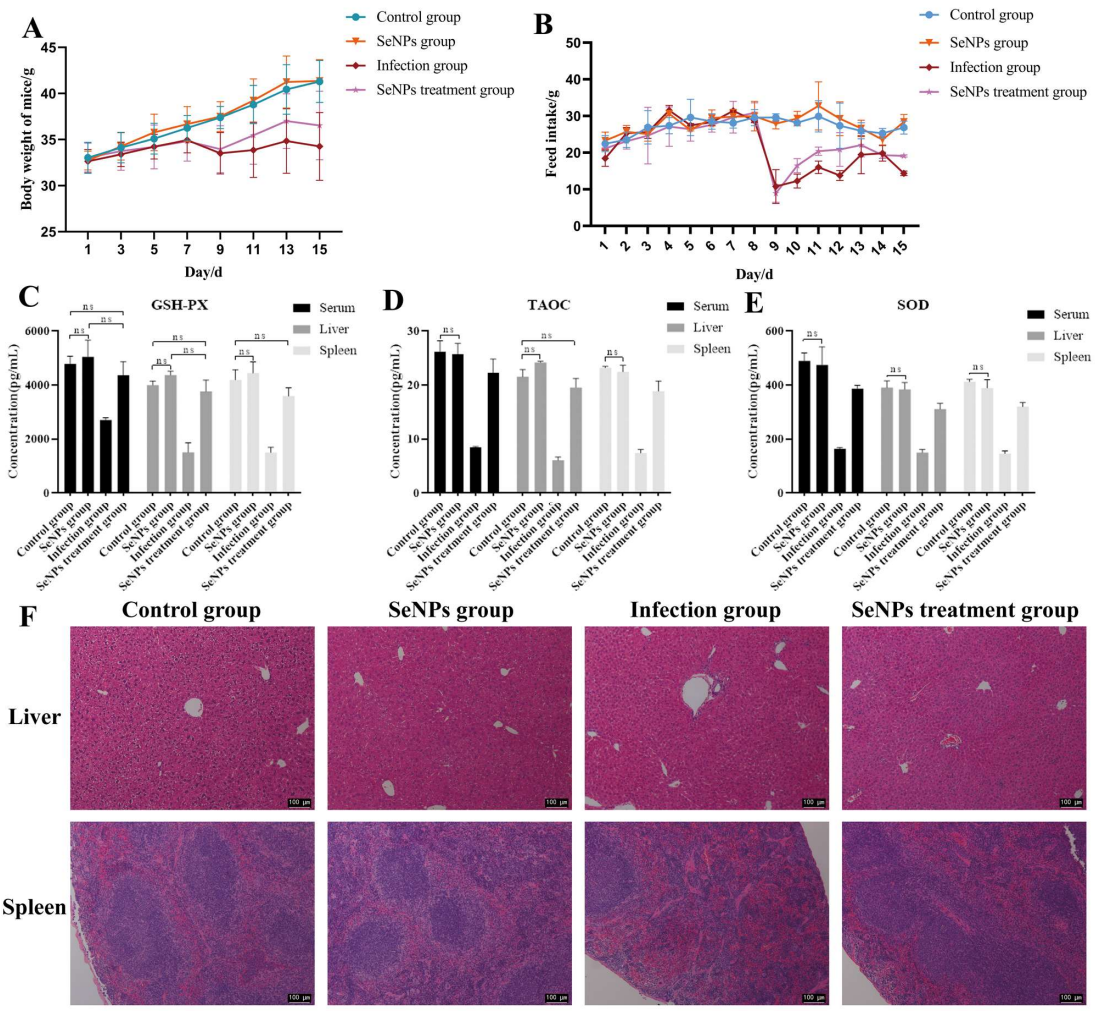

Figure 6. SeNPs mitigate *Streptococcus suis*–induced growth suppression, antioxidant impairment, and liver/spleen injury in mice. (A) Body weight changes over the experimental period. (B) Feed intake over the experimental period. Mice were assigned to four groups: Control , SeNPs, Infection (200 μL *Streptococcus suis*, 1.2×10^9 CFU, injected on Day 8), and SeNPs treatment (oral SeNPs plus infection on Day 8). SeNPs were administered by oral gavage for 15 consecutive days where applicable. (C–E) Antioxidant indices measured at sacrifice in serum, liver, and spleen: GSH-Px (C), total antioxidant capacity (T-AOC; D), and SOD (E). (F) Representative H&E-stained sections of liver (top) and spleen (bottom) from each group. Data are presented as mean ± SD (n = 8 per group). "ns" indicates no significant difference; comparisons without "ns" are significant ($P < 0.05$). Scale bars are shown in the images.

3.7. Transcriptomic Analysis

To elucidate how *Pediococcus acidilactici* JD-21 responds to Se(IV) and supports SeNPs biogenesis, we compared the transcriptomes of selenite-treated cells (Se-JD-21, 5 mmol/L Na_2SeO_3) and untreated controls (JD-21). Under 5 mmol/L selenite, JD-21 exhibited 537 differentially expressed genes (DEGs) relative to the control, including 240 up-regulated and 297 down-regulated genes, indicating extensive transcriptional remodeling under Se(IV) stress (Figure S1). GO and KEGG enrichment analyses showed that up-regulated genes were mainly associated with lipid and fatty acid metabolism, including "lipid biosynthetic/metabolic process", "fatty acid biosynthetic process", "fatty-acid synthase activity", and the KEGG pathway "fatty acid biosynthesis". In parallel, pathways related to cofactor and vitamin metabolism (such as biotin and riboflavin metabolism) and

 doi:10.20944/preprints202606.0122.v1

carbohydrate uptake and utilization were enriched, including amino sugar and nucleotide sugar metabolism, fructose and mannose metabolism, and the phosphotransferase system (PTS) (Figure 7A). Consistent GO terms for cellular polysaccharide/carbohydrate biosynthesis and organic-substance transport were also significantly enriched (Figure 7B). These transcriptional changes resemble those reported in other selenite-reducing bacteria, in which activation of the pentose phosphate pathway (PPP), central carbon metabolism and respiratory/oxidative phosphorylation modules provides NAD(P)H and electron flux required for Se(IV) → Se(0) reduction and SeNPs production[8,31,34]. In JD-21, the concomitant up-regulation of membrane lipid and exopolysaccharide (EPS)-related genes likely supports both the supply of reducing power and the formation of a polysaccharide–protein matrix that facilitates SeNPs nucleation, immobilization and capping, in line with reports that bacterial EPS can stabilize SeNPs and modulate their bioactivity[11,35].

In contrast, down-regulated genes were enriched in processes related to nucleic acid and ribosome modification and replication/maintenance, including rRNA modification/methylation, multiple aminoacyl-tRNA ligase functions, and pyrimidine/UMP/dTDP biosynthesis, as well as KEGG pathways such as “DNA replication”, “mismatch/base-excision/nucleotide-excision repair” and “homologous recombination” (Figure 7C). Additional down-regulated categories involved subsets of amino acid and nitrogen metabolism and transport/secretion functions, including ABC transporters, bacterial secretion systems, two-component systems and quorum sensing (Figure 7D). Overall, these patterns suggest that JD-21 partially reallocates resources from rapid growth and replication toward stress adaptation and detoxification, downshifting energy-intensive processes and selected transport routes while directing reducing equivalents toward Se(IV) reduction and nano-Se biogenesis. This interpretation is consistent with our experimental observations that selenium-enriched JD-21 cells accumulated large amounts of nano-Se and that abundant SeNPs were present both inside and on the surface of the cells, as confirmed by speciation analysis and electron microscopy.

The transcriptomic data also provide clues to transport and redox systems potentially involved in Se(IV) handling. In many bacteria, phosphate and selenite can compete for uptake via low-affinity phosphate transporters such as PitA, so phosphate-transport status can influence Se(IV) entry and intracellular fate[36]. More broadly, ABC, RND and MFS transporters are widely used to export toxic compounds and to remodel membrane traffic under stress, and have been implicated in metal(loid) tolerance in diverse bacteria[37–39]. On the redox side, the SUF Fe–S cluster assembly system is known to function as an oxidative-stress and iron-limitation pathway that maintains Fe–S-dependent biochemistry when prosthetic groups are threatened—a scenario compatible with Se(IV) exposure[40,41]. Catalase-mediated H_2O_2 scavenging is a canonical antioxidant response that helps preserve intracellular redox balance by converting H_2O_2 to water and O_2[42]. Although direct evidence linking catalase up-regulation to enhanced Se(IV) clearance and SeNPs formation remains limited, transcriptomic studies in selenite-tolerant bacteria show coordinated induction of antioxidant and oxidoreductase genes under Se stress, supporting the view that reinforced catalase/oxidoreductase activity can help maintain redox balance and thereby favor efficient Se(IV) reduction and nanoparticle formation[31,34,43]. Finally, several food-grade lactic acid bacteria have been reported to efficiently bioreduce selenite to SeNPs while maintaining high viability[8,44], underscoring the translational relevance of JD-21’s LAB-like response program under Se(IV). Taken together, the JD-21 transcriptome supports a model in which enhanced reducing-power generation, envelope/EPS remodeling and selective transport control are coupled to drive biological selenite reduction and controlled nano-Se deposition.

 doi:10.20944/preprints202606.0122.v1

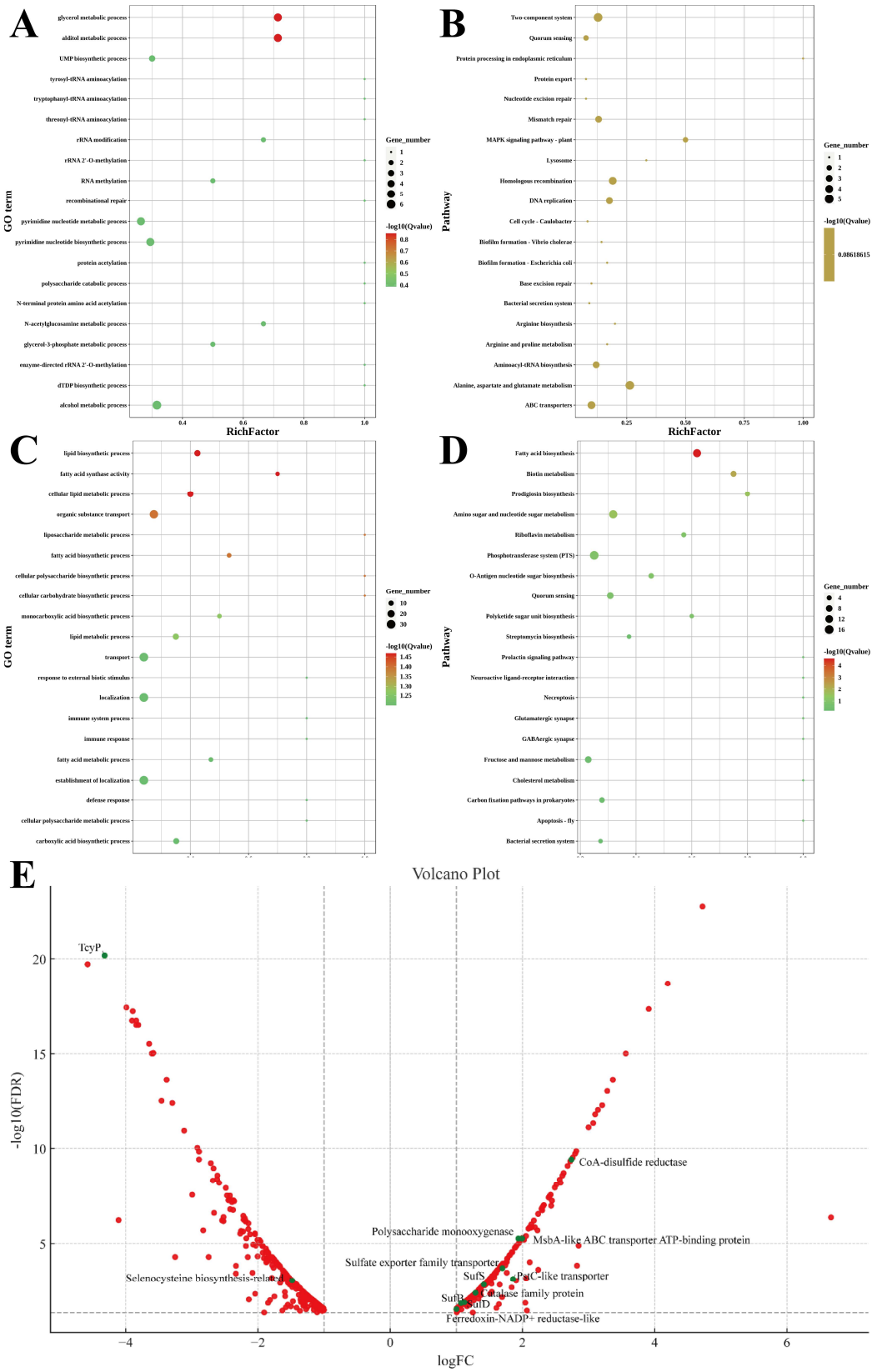

Figure 7. GO (A) and KEGG (B) enrichment of up-regulated genes in *Pediococcus acidilactici* JD-21 under 5 mmol/L sodium selenite (bubble plots). Bubble plots summarizing functional enrichment for genes that were significantly up-regulated in JD-21 under selenite treatment (5 mmol/L Na_2SeO_3) relative to the control. GO (C)

 doi:10.20944/preprints202606.0122.v1

and KEGG (D) enrichment of down-regulated genes in *Pediococcus acidilactici* JD-21 under 5 mmol/L sodium selenite (bubble plots). Bubble plots summarizing functional enrichment for genes that were significantly down-regulated in JD-21 under selenite treatment (5 mmol/LNa_2SeO_3) relative to the control. Left: GO Biological Process terms. Right: KEGG pathways. The x-axis shows the RichFactor (number of up-regulated genes mapped to a term/pathway divided by the total genes annotated to that term/pathway); the y-axis lists the enriched terms/pathways. Bubble size represents the Gene_number (count of mapped up-regulated genes), and bubble color encodes significance as $-\log_{10}$(Q-value) (warmer colors indicate higher significance). These panels provide an overview of functional modules and metabolic routes that are transcriptionally activated under selenite stress. (E) Transcriptomic volcano plot of *Lactobacillus sp*. JD-21 under 5 mmol/L sodium selenite versus control. Volcano plot of differential gene expression under selenite treatment (5 mmol/L Na_2SeO_3) relative to control. The x-axis shows $\log_2$(fold change) and the y-axis shows $-\log_{10}$(FDR). Red circles denote genes with $|\log_2FC|>1$. Vertical dashed lines mark $|\log_2FC|=1$, and the horizontal dashed line marks FDR = 0.05. Green filled circles highlight 12 selenium-relevant genes (labels show gene symbols only): sufS, sufB, sufD, TcyP, sulfate exporter, CoA-disulfide reductase, ferredoxin-$NADP^+$ reductase-like, catalase, MsbA-like ABC, PstC-like, polysaccharide monooxygenase, and selenocysteine biosynthesis-related. These genes are implicated in Fe–S cluster maintenance, sulfur/selenium substrate flux, cellular redox/antioxidant capacity, membrane and transport remodeling, and EPS/envelope processes that collectively support Se(IV) reduction and controlled nano-Se deposition.

3.8. Key Genes Involved in Selenium-Stress Responses

Based on differential expression and functional relevance to selenium metabolism and tolerance, we selected twelve Se-responsive genes for focused discussion (prioritizing $|\log_2FC| > 1$ and/or FDR < 0.05; Figure 7E). Collectively, these genes support a coordinated response to Se(IV) challenge in JD-21, featuring reinforced redox buffering, maintenance of Fe-S homeostasis, selective oxyanion transport, and envelope/EPS remodeling that favors SeNPs formation (Figure 7E).

Transport-related DEGs further indicate that JD-21 modulates selenium flux at the membrane level. A sulfate-exporter–family transporter and a PstC-like phosphate ABC permease were responsive to Se(IV), aligning with evidence that oxyanion transport systems gate selenite entry and speciation. Given the known competition between phosphate and selenite for low-affinity phosphate transport routes (e.g., PitA), remodeling of phosphate/anion transporters is a plausible strategy to tune intracellular Se(IV) burden and downstream fate[36,45,46]. An MsbA-like ABC transporter (lipid flippase/exporter) was also induced, highlighting stress-linked reprogramming of envelope lipid trafficking to preserve membrane integrity and/or facilitate efflux of toxic lipid derivatives during Se(IV) exposure[47–49].

Redox-supporting enzymes were another prominent feature. Coenzyme A-disulfide reductase (CoADR) and a ferredoxin-$NADP^+$ reductase (FNR-like) component were up-regulated, implying reinforcement of NADPH/ferredoxin cycling and low-molecular-weight thiol redox couples. Such changes would help maintain a "reducing budget" for Se(IV) detoxification and SeNPs biogenesis[50–52]. Consistently, catalase showed an increasing trend, supporting the concept that JD-21 activates antioxidant defenses to limit Se(IV)-elicited ROS and protect intracellular redox balance[53].

Finally, genes linked to polysaccharide remodeling and selenium utilization suggest structural and biochemical support for nanoparticle formation. A polysaccharide monooxygenase (PMO-like) was induced, indicating active cell-wall/EPS remodeling under Se stress. Bacterial EPS is widely reported to serve as a capping/stabilizing matrix for biogenic SeNPs, consistent with our FT-IR evidence of protein–polysaccharide coatings and the observed extracellular accumulation of SeNPs[3]. Moreover, a selenocysteine-biosynthesis–related factor was responsive to Se(IV), implying potential engagement of Sec-machinery-associated selenium utilization/detoxification routes in JD-21.

Taken together, these gene-level responses outline a coherent mechanism for JD-21 under Se(IV) stress: (i) preservation of Fe-S clusters and expansion of reducing power (SUF system, CoADR, FNR-

 doi:10.20944/preprints202606.0122.v1

like); (ii) antioxidant containment of ROS (catalase); (iii) transporter-level modulation of selenium/oxyanion influx and efflux (sulfate-exporter family, phosphate transporters, MsbA-like ABC); and (iv) envelope/EPS remodeling that provides a physical matrix for protein-polysaccharide-capped SeNPs. This integrated program is consistent with selenium-reducing bacteria reported previously, while reflecting a LAB-type stress-adaptation mode in JD-21 (Figure 8).

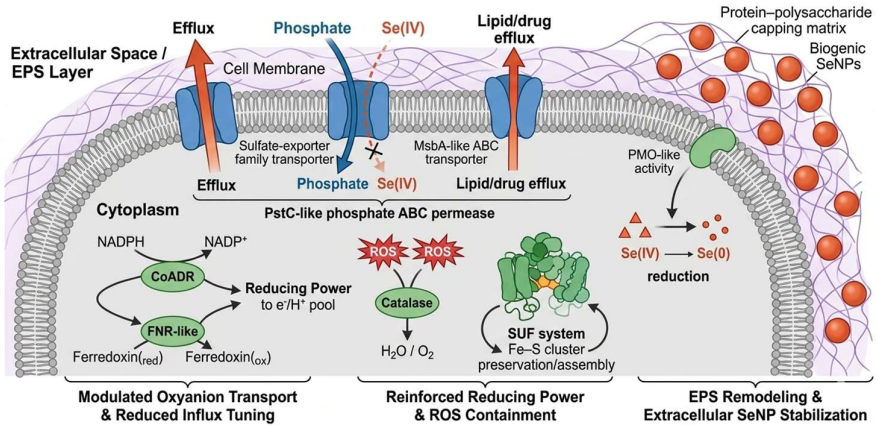

Figure 8. Schematic representation of the integrated molecular mechanism underlying Se(IV) stress response and biogenic selenium nanoparticle (SeNP) formation in strain JD-21. The diagram illustrates a cross-sectional view of the bacterial cell, highlighting four coordinated modules: (i) reinforcement of reducing power and preservation of Fe-S cluster homeostasis via the SUF system, CoADR, and FNR-like components; (ii) activation of antioxidant defenses (e.g., catalase) to contain Se(IV)-induced ROS and maintain intracellular redox balance; (iii) modulation of selenium/oxyanion flux at the membrane level through a sulfate-exporter family transporter, PstC-like phosphate ABC permease, and MsbA-like ABC transporter (lipid flippase/exporter) to tune Se(IV) influx, efflux, and downstream fate; and (iv) envelope and extracellular polymeric substance (EPS) remodeling mediated by a polysaccharide monooxygenase (PMO-like), providing a protein–polysaccharide capping matrix that facilitates nucleation, stabilization, and extracellular accumulation of SeNPs (depicted as orange-red spheres). This multi-layered adaptation program enables efficient Se(IV) detoxification and tolerance in JD-21, consistent with stress-response patterns in selenium-reducing lactic acid bacterium-like strains.

4. Discussion

Microbial reduction of selenite represents an important detoxification strategy and provides a mild biological route for producing elemental selenium nanoparticles (SeNPs). In this study, *Pediococcus acidilactici* JD-21 showed strong Se(IV) tolerance and efficiently converted sodium selenite into red elemental SeNPs, indicating that this strain possesses an effective selenium-stress adaptation system. Compared with many reported lactic acid bacteria, which often tolerate and reduce selenite only at relatively low concentrations, JD-21 showed a stronger ability to survive under Se(IV) stress and accumulate selenium [54]. Selenium speciation, subcellular fractionation and TEM observations collectively suggest that JD-21 preferentially channels Se(IV) toward elemental selenium formation rather than soluble organic selenium accumulation. The major Se(IV)-reducing activity detected in the cytoplasmic fraction supports the view that intracellular reductive reactions are central to SeNP formation, while the presence of SeNPs both inside and outside the cells implies that nanoparticle formation involves reduction, nucleation, intracellular accumulation and subsequent extracellular redistribution or release[55,56].

The characterization of JD-21-derived SeNPs further highlights the advantages of microbial synthesis. TEM showed that the particles were mainly spherical with an average diameter of approximately 60 nm, a size range generally associated with favorable biological activity. FT-IR analysis indicated that the SeNPs were associated with protein- and polysaccharide-like biomolecules, suggesting natural surface capping. Such biomolecular coatings are commonly

 doi:10.20944/preprints202606.0122.v1

reported for biogenic SeNPs and are considered important for improving colloidal stability, reducing aggregation and modulating bioactivity [57,58]. Therefore, the relatively uniform particle morphology and enhanced functional properties observed in this study may be partly attributed to the protein/polysaccharide matrix derived from JD-21 cultures.

Functionally, selenium enrichment markedly strengthened the antibacterial activity of JD-21 against *Escherichia coli*, *Staphylococcus aureus* and *Salmonella enteritidis*, and improved its survival in simulated gastric juice. These effects may result from the combined contribution of SeNPs, selenium-induced metabolic changes and bioactive components produced by JD-21. Similar enhancement of antimicrobial activity after selenium enrichment has been reported in other lactic acid bacteria, supporting the idea that selenium biotransformation can improve the functional performance of probiotic strains [59]. In addition, the improved gastric survival of Se-JD-21 suggests that selenium enrichment may enhance stress resistance, which is important for probiotic application in food and gastrointestinal environments [60].

The in vivo results further suggest that JD-21-derived SeNPs have potential anti-infective activity. In the *Streptococcus suis* infection model, SeNPs administration alleviated infection-associated weight loss and feed-intake reduction, restored T-AOC, SOD and GSH-Px activities, and reduced liver and spleen lesions. These findings are consistent with the well-known role of selenium in antioxidant defense and redox homeostasis[61]. However, this result should be interpreted as preliminary functional evidence rather than a complete mechanism of host protection. The protective effect may involve improved antioxidant capacity, reduced oxidative tissue injury and indirect modulation of inflammatory responses, but these pathways require further validation using inflammatory markers, selenium distribution analysis and dose–response experiments.

Transcriptomic analysis provides a mechanistic framework linking Se(IV) tolerance, SeNP formation and functional enhancement. Under Se(IV) stress, genes related to lipid metabolism, carbohydrate utilization, EPS biosynthesis, cofactor metabolism and redox regulation were up-regulated, while genes associated with DNA replication, repair and growth-related processes were down-regulated. This suggests that JD-21 reallocates cellular resources from rapid growth toward stress adaptation and selenium detoxification. The induction of SUF system genes, CoADR, FNR-like components, catalase and cystine/cysteine transport-related genes indicates reinforcement of Fe–S cluster maintenance, reducing-power supply and antioxidant defense[62,63]. Meanwhile, changes in phosphate/oxyanion transporters and ABC-type transporters may help regulate intracellular selenite flux and maintain membrane homeostasis[64]. EPS- and polysaccharide-related genes may further support SeNP nucleation and surface stabilization, which is consistent with the FT-IR evidence of protein/polysaccharide capping.

Despite these findings, several limitations should be acknowledged. First, the transcriptomic results identify candidate pathways and genes associated with Se(IV) stress, but their specific functions in SeNP biosynthesis remain to be experimentally validated. Targeted gene knockout, overexpression or enzyme assays are needed to confirm their roles. Second, although SeNPs showed promising anti-infective activity in mice, long-term safety, bioavailability and dose-dependent effects were not fully evaluated. Third, the performance of JD-21-derived SeNPs or selenium-enriched biomass in real food matrices remains unclear. Future studies should therefore focus on mechanism validation, fermentation optimization, product stability, selenium bioavailability and application evaluation in food systems.

5. Conclusions

A highly Se(IV)-tolerant lactic acid bacteria, *Pediococcus acidilactici* JD-21 (CCTCC M 20241452), was isolated and shown to withstand up to 100 mmol/L selenite and efficiently reduce Se(IV) at 5 mmol/L. JD-21 accumulated selenium mainly as elemental SeNPs. Reduction activity was primarily localized to the cytoplasmic fraction, and TEM revealed abundant spherical SeNPs (~60 nm) distributed intra- and extracellularly. FT-IR indicated that these biogenic SeNPs were naturally capped by protein- and polysaccharide-like biomolecules, suggesting intrinsic stabilization.

 doi:10.20944/preprints202606.0122.v1

Selenium enrichment markedly improved strain functionality: Se-JD-21 showed enhanced antibacterial activity against *E. coli*, *S. aureus*, and *S. enteritidis*, and higher survival in simulated gastric juice, supporting probiotic potential. *In vivo*, SeNPs administration alleviated *Streptococcus suis* infection–associated weight loss and anorexia, restored antioxidant enzyme activities (T-AOC, SOD, GSH-Px), and reduced liver/spleen lesions without obvious toxicity. Transcriptomics revealed a coordinated Se(IV) response featuring upregulated reducing-power generation, lipid/EPS remodeling, and selective transport control, alongside downregulation of growth-related processes, and highlighted key genes (e.g., SUF system, CoADR, transporters, catalase, EPS-related factors) underpinning SeNP formation and tolerance.

Supplementary Materials: The following supporting information can be downloaded at the website of this paper posted on Preprints.org, Figure S1: Integrated overview of the transcriptomic workflow and DEG landscape of *Pediococcus acidilactici* JD-21 under 5 mM selenite. (A) Transcriptomic Analysis Workflow for JD-21 Selenium Tolerance Mechanism. Workflow Overview: This flowchart illustrates the sequential steps involved in analyzing the transcriptomic response of JD-21 strain to selenium treatment. It begins with strain cultivation and branches into experimental (selenium-treated) and control groups. The process then converges through RNA extraction, sequencing data generation, and bioinformatics analysis steps, culminating in functional annotation and differential expression analysis. (B) Differentially expressed genes (DEGs) in JD-21 under 5 mM selenite vs control: counts of Up and Down. Bar chart summarizing the numbers of down-regulated and up-regulated genes for the A-vs-B comparison (JD-21, 5 mM Na_2SeO_3 vs control). The y-axis shows the number of DEGs; blue indicates Down (297; 55.3%) and red indicates Up (240; 44.7%). Values and percentages are annotated above each bar. This panel provides an overview of the transcriptional directionality prior to enrichment analyses; Table S1:Working parameters of HPLC and ICP-MS.

Author Contributions: Shiyue Fan: Writing – original draft, Visualization, Methodology, Data curation and Investigation. Jiaxu Li: Visualization, Methodology, Data curation and Investigation. Xin Zhao: Validation, Methodology, Investigation. Yi He: Writing – review and editing, Funding acquisition, Conceptualization. Zhiwei Li: Methodology, Writing - review and editing. Zhangqian Wang and Chao Gao and Ying Ma: Validation, Methodology. Jinquan Li: Writing – review and editing. Xiaoling Chen: Methodology, Investigation. Wen Cheng: Conceptualization, Funding acquisition. Xingxing Dong: Conceptualization, Writing - review and editing, Resources, Supervision, Funding acquisition and Project administration. All authors have read and agreed to the published version of the manuscript.

Funding: This work was supported by the Enterprise Joint Technology R&D Project (No. 02224191), the Outstanding Youth Program of Hubei Provincial Natural Science Foundation (No. 2023AFA102), and the Hubei Provincial Natural Science Foundation Project (No. 2022CFB945).

Institutional Review Board Statement: The animal study protocol was approved by the Animal Ethics Committee of Wuhan Myhalic Biotechnology Co., Ltd (protocol code HLK 20230921-004, Sep 21, 2023).

Informed Consent Statement: Not applicable.

Data Availability Statement: The transcriptomic (RNA-seq) data generated in this study have been deposited in GenBank under the BioProject accession number PRJNA1372184. All other data supporting the findings of this work are available from the corresponding author upon reasonable request.

Acknowledgments: During the preparation of this manuscript, the authors used ChatGPT (OpenAI) to assist with English language polishing, structural refinement, and improvement of clarity and readability. The tool was not used to generate experimental data, perform statistical analyses, create original scientific conclusions, or replace the authors' interpretation of the results. All AI-assisted content was carefully reviewed, edited, and verified by the authors, who take full responsibility for the content of the manuscript.

Conflicts of Interest: The authors declare that they have no known competing financial interests or personal relationships that could have appeared to influence the work reported in this paper. The funders had no role in

 doi:10.20944/preprints202606.0122.v1

the design of the study; in the collection, analyses, or interpretation of data; in the writing of the manuscript; or in the decision to publish the results.

References

1. Nan, C.; Peng, Y.; Wei, Z.; Yutong, Z.; Naicheng, X.; Hongdi, W.; Tiehua, Z.; Changhui, Z. Selenium nanoparticles: Enhanced nutrition and beyond. %J Critical reviews in food science and nutrition. **2022**, *63*, 11-12, doi:10.1080/10408398.2022.2101093.
2. Xianli, G.; Chao, Y.; Haile, M.; Zhankai, Z.; Jiacheng, W.; ZhiHong, Z.; Xue, Z.; ChiTang, H. Research Advances in Preparation, Stability, Application, and Possible Risks of Nanoselenium: Focus on Food and Food-Related Fields. %J Journal of agricultural and food chemistry. **2023**, *71*, doi:10.1021/acs.Jafc.3c02714.
3. Olena, S.; Myroslav, K.; Iryna, K.; Viktor, S. Biosynthesis of selenium nanoparticles by lactic acid bacteria and areas of their possible applications. %J World journal of microbiology & biotechnology. **2023**, *39*, 230-230, doi:10.1007/s11274-023-03673-6.
4. Dan, W.; Christopher, R.; Shixue, Z. Microbial reduction and resistance to selenium: Mechanisms, applications and prospects %J Journal of Hazardous Materials. **2022**, *421*, 126684-126684, doi:10.1016/j.Jhazmat.2021.126684.
5. Hong, C.; Gengan, D.; Xiaohai, Y.; Huanfeng, Y.; Qi, G.; Zhouli, W.; Yahong, Y.; Tianli, Y. Selenium-Enriched Pediococcus acidilactici MRS-7 Alleviates Patulin-Induced Jejunum Injuries in Mice and Its Possible Mechanisms. *Journal of agricultural and food chemistry* **2022**, *70*, doi:10.1021/acs.Jafc.2c00949.
6. Francisco, Y.; Rubén, M.; T., S.C.; Paulina, A.; Kimberly, S.; Apolinaria, G.; Ariel, V.; L., C.V. Selenium Nanoparticle-Enriched and Potential Probiotic, Lactiplantibacillus plantarum S14 Strain, a Diet Supplement Beneficial for Rainbow Trout %J Biology. **2022**, *11*, 1523-1523, doi:10.3390/biology11101523.
7. Bo, A.; Qingquan, D.; Decheng, L.; Xiaoshan, S.; Junming, T.; Xian, X. A review on synthesis and antibacterial potential of bio-selenium nanoparticles in the food industry. *Frontiers in microbiology* **2023**, *14*, 1229838-1229838, doi:10.3389/fmicb.2023.1229838.
8. Lei, Q.; Xina, D.; Xiaofan, S.; Jiajing, C.; Xiaonan, Z.; Lixu, Z.; Chunlan, X. Selenite Bioremediation by Food-Grade Probiotic Lactobacillus casei ATCC 393: Insights from Proteomics Analysis. %J Microbiology spectrum. **2023**, *11*, e0065923-e0065923, doi:10.1128/spectrum.00659-23.
9. Wang, L.; Song, L.; Wang, P.; Zhang, H.; Li, Y.; Song, J.; Zhong, L.; Liu, C.; Zhang, W.; Wen, P. Bioreduction of Se(IV) by Lactiplantibacillus plantarum NML21 and synthesis of selenium nanospheres Se(0). %J Food chemistry. **2024**, *452*, 139595-139595, doi:10.1016/j.Foodchem.2024.139595.
10. ZhiJian, L.; QingQing, W.; FuJuan, D.; HaiFeng, L. Reduction of selenite to selenium nanospheres by Se(IV)-resistant Lactobacillus paralimentarius JZ07 %J Food Chemistry. **2022**, *393*, 133385-133385, doi:10.1016/j.Foodchem.2022.133385.
11. S., S.N.; H., E.B.; S., E.S.; A., G.D.; A., O.Z. Selenium nanoparticles coated bacterial polysaccharide with potent antimicrobial and anti-lung cancer activities %J Scientific Reports. **2023**, *13*, 21871-21871, doi:10.1038/s41598-023-48921-9.
12. Shehata, N.S.; Elwakil, B.H.; Elshewemi, S.S.; Ghareeb, D.A.; Olama, Z.A. In vitro and in vivo studies of selenium nanoparticles coated bacterial polysaccharide as anti-lung cancer agents %J Microbial Cell Factories. **2024**, *23*, 339-339, doi:10.1186/s12934-024-02601-z.
13. Hong, C.; Xiaoyu, W.; Yuan, Y.; Xin, W.; Xuejun, Z.; Qi, G.; Xiaohai, Y.; Gengan, D.; Yahong, Y.; Tianli, Y. Enrichment and Distribution of Selenium in Pediococcus acidilactici MRS-7: Impact on Its Biochemical Composition, Microstructure, and Gastrointestinal Survival. %J Journal of agricultural and food chemistry. **2022**, doi:10.1021/acs.Jafc.2c06765.
14. Rui, W.; Sun, Y.; Li, X.; Yang, J.; Tang, X. Selenium-Enriched Akkermansia muciniphila: A Novel Probiotic Bacterium for Se Supplementation. %J Probiotics and antimicrobial proteins. **2025**, 1-15, doi:10.1007/s12602-025-10713-0.
15. Zhong, B.; Xu, W.; Gong, M.; Xian, W.; Xie, H.; Wu, Z. Molecular mechanisms of selenite reduction by Lactiplantibacillus plantarum BSe: An integrated genomic and transcriptomic analysis. %J Journal of hazardous materials. **2024**, *468*, 133850-133850, doi:10.1016/j.Jhazmat.2024.133850.

 doi:10.20944/preprints202606.0122.v1

16. Liu, X.; Mao, Y.; Huang, S.; Li, W.; Zhang, W.; An, J.; Jin, Y.; Guan, J.; Wu, L.; Zhou, P. Selenium nanoparticles derived from Proteus mirabilis YC801 alleviate oxidative stress and inflammatory response to promote nerve repair in rats with spinal cord injury. *Regenerative biomaterials* **2022**, *9*, rbac042, doi:10.1093/rb/rbac042.
17. Qiao, L.; Zhang, X.; Pi, S.; Chang, J.; Dou, X.; Yan, S.; Song, X.; Chen, Y.; Zeng, X.; Zhu, L.; et al. Dietary supplementation with biogenic selenium nanoparticles alleviate oxidative stress-induced intestinal barrier dysfunction. *NPJ science of food* **2022**, *6*, 30, doi:10.1038/s41538-022-00145-3.
18. Abdel-Gaber, R.; Hawsah, M.A.; Al-Otaibi, T.; Alojayri, G.; Al-Shaebi, E.M.; Mohammed, O.B.; Elkhadragy, M.F.; Al-Quraishy, S.; Dkhil, M.A. Biosynthesized selenium nanoparticles to rescue coccidiosis-mediated oxidative stress, apoptosis and inflammation in the jejunum of mice. *Front Immunol* **2023**, *14*, 1139899, doi:10.3389/fimmu.2023.1139899.
19. Palomo-Siguero, M.; Madrid, Y. Exploring the Behavior and Metabolic Transformations of SeNPs in Exposed Lactic Acid Bacteria. Effect of Nanoparticles Coating Agent. *International Journal of Molecular Sciences* **2017**, *18*, 1712-1712, doi:10.3390/ijms18081712.
20. Yinglian, Z.; Yuning, X.; Qingli, Y. Antifungal properties and AFB1 detoxification activity of a new strain of Lactobacillus plantarum %J Journal of Hazardous Materials. **2021**, *414*, 125569-125569, doi:10.1016/j.Jhazmat.2021.125569.
21. Qing, H.; Wei, L.; XinQuan, Y.; DongXiao, S.; Shan, H.; Anindya, N.; QingZhu, Z.; Yang, Y. Development, characterization and in vitro bile salts binding capacity of selenium nanoparticles stabilized by soybean polypeptides. %J Food chemistry. **2022**, *391*, 133286-133286, doi:10.1016/j.Foodchem.2022.133286.
22. Liu, L.; Yang, S.; Wang, R.; Li, S.; Qi, J.; Wang, L.; Yue, T.; Wang, Z.; Yuan, Y. Characterization and subcellular localization of selenium in Limosilactobacillus fermentum Ln-9 obtained by intense pulsed light-ultraviolet combined mutagenesis. %J Food chemistry. **2024**, *460*, 140725, doi:10.1016/j.Foodchem.2024.140725.
23. Yang, J.; Qiuhui, H.; Gaoxing, M.; Anqi, Y.; Liyan, Z.; Xueli, Z.; Ruiqiu, Z. Selenium biofortification in Pleurotus eryngii and its effect on lead adsorption of gut microbiota via in vitro fermentation %J Food Chemistry. **2022**, *396*, 133664-133664, doi:10.1016/j.Foodchem.2022.133664.
24. Zan, L.; Chen, Z.; Zhang, B.; Zou, X.; Lan, A.; Zhang, W.; Yuan, Y.; Yue, T. Screening, Characterization and Probiotic Properties of Selenium-Enriched Lactic Acid Bacteria. *Fermentation* **2024**, *10*, doi:10.3390/fermentation10010039.
25. Yuheng, H.; Yan, X.; Qingtai, S.; Jiahao, F.; Jialu, C.; Yanan, L. Probiotic and Safety Evaluation of Twelve Lactic Acid Bacteria as Future Probiotics. *Foodborne pathogens and disease* **2023**, *20*, 521-530, doi:10.1089/fpd.2023.0039.
26. Zahra, E.; Bahareh, V.; Shahrzah, A.; Nasr, E.S.; Parisa, S. Impact of Selenium Nanoparticle-Enriched Lactobacilli Feeding Against Escherichia coli O157:H7 Infection of BALB/c Mice. *Probiotics and antimicrobial proteins* **2023**, *16*, 784-795, doi:10.1007/s12602-023-10081-7.
27. Huiling, J.; Shengwei, H.; Shuo, C.; Xiwen, Z.; Xue, C.; Yisen, Z.; Jun, W.; Lifang, W. Novel mechanisms of selenite reduction in Bacillus subtilis 168：Confirmation of multiple-pathway mediated remediation based on transcriptome analysis. %J Journal of hazardous materials. **2022**, *433*, 128834-128834, doi:10.1016/j.Jhazmat.2022.128834.
28. Qingdong, W.; Chunyue, W.; Shanshan, K.; Dezhen, W.; Yuhua, S. Biological Selenite Reduction, Characterization and Bioactivities of Selenium Nanoparticles Biosynthesised by Pediococcus acidilactici DSM20284. %J Molecules (Basel, Switzerland). **2023**, *28*, doi:10.3390/molecules28093793.
29. Jingpeng, Y.; Hong, Y. Recent development in Se-enriched yeast, lactic acid bacteria and bifidobacteria. *Critical reviews in food science and nutrition* **2021**, *63*, 11-15, doi:10.1080/10408398.2021.1948818.
30. Li, R.; Chen, W.; Huang, S.; Jiang, D.; Zhu, Z.; Li, C.; Huang, X. Three bacterial strains efficiently reduce selenite to selenium nanoparticles in cell membranes. *BMC Microbiology* **2025**, *25*, 564-564, doi:10.1186/s12866-025-04304-w.
31. original/au/au-aff. Speeding up selenite bioremediation using the highly selenite-tolerant strain Providencia rettgeri HF16-A novel mechanism of selenite reduction based on proteomic analysis %J Journal of Hazardous Materials. **2021**, *406*, doi:10.1016/j.jhazmat.2020.124690.

 doi:10.20944/preprints202606.0122.v1

32. Yang, J.; Wang, J.; Yang, K.; Liu, M.; Qi, Y.; Zhang, T.; Fan, M.; Wei, X. Antibacterial activity of selenium-enriched lactic acid bacteria against common food-borne pathogens in vitro. *Journal of Dairy Science* **2018**, *101*, 1930-1942, doi:10.3168/jds.2017-13430.
33. Lv, C.; Pang, X.; Sun, J.; Li, X.; Lu, Y. Screening of bile salt hydrolase-producing lactic acid bacteria and evaluation of cholesterol-lowering activity in vitro. *Food Bioscience* **2024**, *62*, 105338-105338, doi:10.1016/j.Fbio.2024.105338.
34. Yuting, W.; Qing, Y.; Yujun, S.; Yulu, J.; Bo, M.; Jun, D.; Jingjing, C.; V., T.A.; A., K.A.; Shengwei, H. Selenite Reduction by Proteus sp. YS02: New Insights Revealed by Comparative Transcriptomics and Antibacterial Effectiveness of the Biogenic Se0 Nanoparticles
 %J Frontiers in Microbiology. **2022**, *13*, 845321-845321, doi:10.3389/fmicb.2022.845321.
35. Ramachandran, T.; Manoharan, D.; Natesan, S.; Rajaram, S.K.; Karuppiah, P.; Shaik, M.R.; Khan, M.; Shaik, B. Synthesis and Structural Characterization of Selenium Nanoparticles– Bacillussp. MKUST-01 Exopolysaccharide (SeNPs–EPS) Conjugate for Biomedical Applications %J Biomedicines. **2023**, *11*, doi:10.3390/biomedicines11092520.
36. Ting, Z.T.; Jiao, T.L.; Qing, Y.H. Phosphate-Suppressed Selenite Biotransformation by Escherichia coli. %J Environmental science & technology. **2020**, *54*, doi:10.1021/acs.est.0c02175.
37. Jacek, L.; N, K.W.; M, D.A.J. Distribution and physiology of ABC-type transporters contributing to multidrug resistance in bacteria. %J Microbiology and molecular biology reviews : MMBR. **2007**, *71*, 463-476.
38. Lu, M.; Jiao, S.; Gao, E.; Song, X.; Li, Z.; Hao, X.; Rensing, C.; Wei, G. Transcriptome Response to Heavy Metals in Sinorhizobium meliloti CCNWSX0020 Reveals New Metal Resistance Determinants That Also Promote Bioremediation by Medicago lupulina in Metal-Contaminated Soil %J Appl. Environ. Microbiol. **2017**, *83*, e01244-01217, doi:10.1128/aem.01244-17.
39. Hongshi, X.; Jun, T.; Mengjia, L.; Zhihui, Y.; Haiyan, Z. The mechanism of Se(IV) multisystem resistance in Stenotrophomonas sp. EGS12 and its prospect in selenium-contaminated environment remediation. %J Journal of hazardous materials. **2023**, *452*, 131358-131358, doi:10.1016/j.Jhazmat.2023.131358.
40. Chemistry, D.o.; Biochemistry, U.o.S.C., 631 Sumter Street, Columbia, SC 29208, USA; Chemistry, D.o.; Biochemistry, U.o.S.C., 631 Sumter Street, Columbia, SC 29208, USA; Chemistry, D.o.; Biochemistry, U.o.S.C., 631 Sumter Street, Columbia, SC 29208, USA; Chemistry, D.o.; Biochemistry, U.o.S.C., 631 Sumter Street, Columbia, SC 29208, USA. Fe-S cluster biogenesis by the bacterial Suf pathway. *BBA - Molecular Cell Research* **2020**, *1867*, 118829-118829, doi:10.1016/j.bbamcr.2020.118829.
41. Outten, F.W. Recent advances in the Suf Fe–S cluster biogenesis pathway: Beyond the Proteobacteria %J BBA - Molecular Cell Research. **2015**, *1853*, 1464-1469, doi:10.1016/j.bbamcr.2014.11.001.
42. Fang, Y.; Shouliang, Y.; Yang, X.; Lijun, X.; Haiyan, W.; Zilong, L.; Keqiang, F.; Guohui, P. The Richness and Diversity of Catalases in Bacteria
 %J Frontiers in Microbiology. **2021**, *12*, 645477-645477, doi:10.3389/fmicb.2021.645477.
43. Ge, M.; Zhou, S.; Li, D.; Song, D.; Yang, S.; Xu, M. Reduction of selenite to selenium nanoparticles by highly selenite-tolerant bacteria isolated from seleniferous soil. %J Journal of hazardous materials. **2024**, *472*, 134491-134491, doi:10.1016/j.Jhazmat.2024.134491.
44. Gabriel, M.F.; Gustavo, M.-M.; Micaela, P.; Yolanda, M.-A.; Fernanda, M. Biotransformation of Selenium by Lactic Acid Bacteria: Formation of Seleno-Nanoparticles and Seleno-Amino Acids. %J Frontiers in bioengineering and biotechnology. **2020**, *8*, 506, doi:10.3389/fbioe.2020.00506.
45. Myriam, L.; Sylvain, B.; Paola, F.; Guillaume, L.; Pierre, P. Uptake of selenite by Saccharomyces cerevisiae involves the high and low affinity orthophosphate transporters. %J The Journal of biological chemistry. **2010**, *285*, 32029-32037, doi:10.1074/jbc.M110.139865.
46. K, V.R.; R, H.C.; P, S.K.A.; M, K.K.; R, M.W. Phosphate signaling through alternate conformations of the PstSCAB phosphate transporter. %J BMC microbiology. **2018**, *18*, 8, doi:10.1186/s12866-017-1126-z.
47. L, R.C.; Andrew, W.; Jodie, Y.; Geoffrey, C. The structures of MsbA: Insight into ABC transporter-mediated multidrug efflux. %J FEBS letters. **2006**, *580*, 1042-1048.

 doi:10.20944/preprints202606.0122.v1

48. Jixing, L.; Chang, L.; Tianqi, Z.; Samantha, S.; P., E.N.; Charles, P.; A., H.G.K.; David, R.; Minglei, Z.; Arthur, L. Structural basis for lipid and copper regulation of the ABC transporter MsbA %J Nature Communications. **2022**, *13*, 7291-7291, doi:10.1038/s41467-022-34905-2.
49. Bisht, R.; Charlesworth, P.D.; Sperandeo, P.; Polissi, A. Breaking Barriers: Exploiting Envelope Biogenesis and Stress Responses to Develop Novel Antimicrobial Strategies in Gram-Negative Bacteria %J Pathogens. **2024**, *13*, 889-889, doi:10.3390/pathogens13100889.
50. delCardayre, S.B.; Stock, K.P.; Newton, G.L.; Fahey, R.C.; Davies, J.E. Coenzyme A disulfide reductase, the primary low molecular weight disulfide reductase from Staphylococcus aureus. Purification and characterization of the native enzyme. *The Journal of biological chemistry* **1998**, *273*, 5744-5751, doi:10.1074/jbc.273.10.5744.
51. Ivan, G. Coenzyme A: a protective thiol in bacterial antioxidant defence. %J Biochemical Society transactions. **2019**, *47*, 469-476, doi:10.1042/bst20180415.
52. Conn, M.T.; R, W.J.; Andrew, K.P.; Hiroaki, S.; Tomitake, T.; Al, C. Structure of coenzyme A-disulfide reductase from Staphylococcus aureus at 1.54 A resolution. %J Biochemistry. **2006**, *45*, 11278-11289.
53. Magali, B.; Gilles, L.; Jérôme, G.; Danièle, T.; André, V.; Jean, L. Involvement of superoxide dismutases in the response of Escherichia coli to selenium oxides. %J Journal of bacteriology. **2002**, *184*, 1556-1564, doi:10.1128/jb.184.6.1556-1564.2002.
54. Stabnikova, O.; Khonkiv, M.; Kovshar, I.; Stabnikov, V. Biosynthesis of selenium nanoparticles by lactic acid bacteria and areas of their possible applications. *World J Microbiol Biotechnol* **2023**, *39*, 230, doi:10.1007/s11274-023-03673-6.
55. Huang, S.; Wang, Y.; Tang, C.; Jia, H.; Wu, L. Speeding up selenite bioremediation using the highly selenite-tolerant strain Providencia rettgeri HF16-A novel mechanism of selenite reduction based on proteomic analysis. *Journal of hazardous materials* **2021**, *406*, 124690, doi:10.1016/j.jhazmat.2020.124690.
56. Wang, Y.; Ye, Q.; Sun, Y.; Jiang, Y.; Meng, B.; Du, J.; Chen, J.; Tugarova, A.V.; Kamnev, A.A.; Huang, S. Selenite Reduction by Proteus sp. YS02: New Insights Revealed by Comparative Transcriptomics and Antibacterial Effectiveness of the Biogenic Se(0) Nanoparticles. *Front Microbiol* **2022**, *13*, 845321, doi:10.3389/fmicb.2022.845321.
57. Shehata, N.S.; Elwakil, B.H.; Elshewemi, S.S.; Ghareeb, D.A.; Olama, Z.A. Selenium nanoparticles coated bacterial polysaccharide with potent antimicrobial and anti-lung cancer activities. *Sci Rep* **2023**, *13*, 21871, doi:10.1038/s41598-023-48921-9.
58. Concordio-Reis, P.; Macedo, A.C.; Cardeira, M.; Moppert, X.; Guezennec, J.; Sevrin, C.; Grandfils, C.; Serra, A.T.; Freitas, F. Selenium Bio-Nanocomposite Based on Alteromonas macleodii Mo169 Exopolysaccharide: Synthesis, Characterization, and In Vitro Antioxidant Activity. *Bioengineering* **2023**, *10*, doi:10.3390/bioengineering10020193.
59. Yang, J.; Wang, J.; Yang, K.; Liu, M.; Qi, Y.; Zhang, T.; Fan, M.; Wei, X. Antibacterial activity of selenium-enriched lactic acid bacteria against common food-borne pathogens in vitro. *Journal of dairy science* **2018**, *101*, 1930-1942, doi:10.3168/jds.2017-13430.
60. Corcoran, B.M.; Stanton, C.; Fitzgerald, G.F.; Ross, R.P. Survival of probiotic lactobacilli in acidic environments is enhanced in the presence of metabolizable sugars. *Appl Environ Microbiol* **2005**, *71*, 3060-3067, doi:10.1128/AEM.71.6.3060-3067.2005.
61. Du, H.; Zheng, Y.; Zhang, W.; Tang, H.; Jing, B.; Li, H.; Xu, F.; Lin, J.; Fu, H.; Chang, L.; et al. Nano-Selenium Alleviates Cadmium-Induced Acute Hepatic Toxicity by Decreasing Oxidative Stress and Activating the Nrf2 Pathway in Male Kunming Mice. *Front Vet Sci* **2022**, *9*, 942189, doi:10.3389/fvets.2022.942189.
62. Blahut, M.; Sanchez, E.; Fisher, C.E.; Outten, F.W. Fe-S cluster biogenesis by the bacterial Suf pathway. *Biochimica et biophysica acta. Molecular cell research* **2020**, *1867*, 118829, doi:10.1016/j.bbamcr.2020.118829.
63. Outten, F.W. Recent advances in the Suf Fe-S cluster biogenesis pathway: Beyond the Proteobacteria. *Biochimica et biophysica acta* **2015**, *1853*, 1464-1469, doi:10.1016/j.bbamcr.2014.11.001.
64. Zhu, T.T.; Tian, L.J.; Yu, H.Q. Phosphate-Suppressed Selenite Biotransformation by Escherichia coli. *Environ Sci Technol* **2020**, *54*, 10713-10721, doi:10.1021/acs.est.0c02175.

 doi:10.20944/preprints202606.0122.v1